Conference Proceedings 4th ICTB (2022)
https://doi.org/10.24451/gak8-4k79

ICTB 2021 PLUS
4th International Conference on Timber Bridges
Biel/Bienne, Switzerland, 9 -12 May 2022

Study of the dynamic response of a timber pedestrian bridge during different construction stages

Jens Bergenudd[1], Jean-Marc Battini, Roberto Crocetti, Costin Pacoste

Abstract

The objective of this article is to study the dynamic behaviour of a timber pedestrian bridge by performing in-situ tests at four different construction stages: 1) on only the timber structure 2) on the timber structure with the railings 3) on the timber structure with railings and an asphalt layer during warm conditions and 4) same as stage 3 but during cold conditions. The study included numerical calculations with a 2D finite element model. Two modal parameter extraction methods were implemented during the post-processing. The modes of vibration were analysed with the modal assurance criterion (MAC) to ensure their validity. The results show that the presence of the railings during stage 2 increases the resonance frequencies with 0-2 % compared to stage 1, despite an approximately 5 % increase of the total mass of the bridge. The vertical resonance frequencies decreased 12-22 % when the asphalt was installed at stage 3 compared to stage 2, due to an approximately 70 % increase of the total mass and the asphalt's low stiffness due to a high temperature. The resonance frequencies increased 14-27 % during cold conditions at stage 4 compared to stage 3. This was mainly due to an increased stiffness of the asphalt layer due to a low temperature. Adding railings therefore resulted in a higher overall stiffness of the bridge, whereas asphalt essentially only added mass to the bridge at warm conditions but increased the stiffness at cold compared to warm conditions. The damping ratios increased for each construction stage and were approximately 2-3 % for the finished bridge. The two modal parameter extraction methods produced similar results which ensures that reliable results are obtained. The auto-MAC indicated well-separated modes and the cross-MAC ensured comparison of the same modes. The finite element model showed that some stiffness was lacking for the first bending mode. This stiffness could be due to shear deformation of the plastic pads at the bridge supports.

1 Introduction

Timber is a sustainable construction material and is suitable for short and medium span bridges, particularly pedestrian bridges. This is beneficial in areas with high availability of timber and with fairly short transports. Parts of the bridges can also be assembled in a factory and lifted in place on-site which reduces the construction time [1]. Problems with vibrations can however be a problem for these bridges since they can be made quite slender [2]–[5]. Therefore, it is important to have adequate calculation models in the design phase.

As a way to reach more refined finite element (FE) models for timber pedestrian bridges, a research project has been initiated where a number of bridges will be dynamically tested during different construction stages and at different seasons to study temperature effects. In this way, the influence of the different parts of the bridge, such as railings and an asphalt layer, can be identified. The asphalt stiffness is for example highly temperature dependent and has been reported to lower the resonance frequencies at warm temperatures and vice versa. Asphalt also increases damping which is mainly due to friction at the interface between timber deck and asphalt as well as internal viscous friction [6], [7].

A timber pedestrian bridge in Växjö, Sweden, has been investigated during four different construction stages. The main objective was to study the difference of the resonance frequencies and damping ratios. The modes of vibration were also compared and investigated for the different construction stages. Two modal parameter extraction methods were implemented during the post-processing to achieve reliable results and to investigate their interchangeability.

[1] Jens Bergenudd, PhD student, Department of Civil and Architectural Engineering, KTH, Royal Institute of Technology, Stockholm, Sweden, jbergenu@kth.se

2 Material and method

This section describes the bridge, the experimental tests and the methods to post-process the experimental data.

2.1 The bridge

The bridge is a single-span pedestrian timber bridge situated in Växjö, Sweden, see Figure 1. The bridge is 26.1 m long in total with a span of 25 m. The loadbearing structure consists of five longitudinal glulam beams (165x1170 mm) with a top flange made of a stress-laminated timber (SLT) deck with a thickness of 315 mm and total width of 4005 mm, see Figure 2. The connection between the SLT deck at the top flange and the longitudinal beams is achieved with friction due to the pre-stressing force from 43 steel bars running through the deck. Five crossbeams (115x540 mm) are installed at 5 locations between the longitudinal beams with a c/c of 6 m along the bridge. The crossbeams are connected to the longitudinal beams with angle irons. Steel bars also are installed at the lower flange of the longitudinal beams at the same locations as the crossbeams to prevent lateral deflection of the longitudinal beams. All the structural timber parts of the bridge are made of glulam with strength class GL30c. The finished bridge have railings which extend 7.65 m from the bridge deck boundary edges as well as an asphalt layer with a constant thickness of 75 mm. The asphalt layer is a preliminary layer without the final camber with a 2 % slope seen in Figure 2. The asphalt is termed PGJA 11 in the Swedish norm which consists of mastic asphalt (MA) with a nominal maximal aggregate size of 11 mm and polymer modified bitumen (PMB).

Figure 1: An overview of the finished bridge.

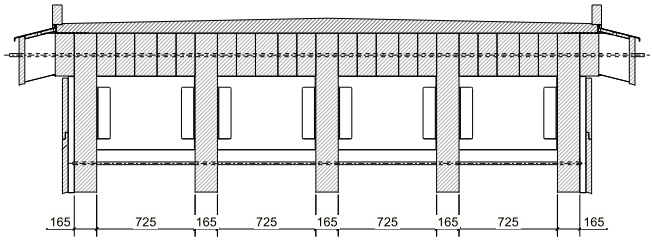

Figure 2: The bridge cross-section. Dimensions are in mm.

2.2 Equipment

Nineteen accelerometers of type PCB 393a03 with a sensitivity of 1 V/g were placed on the bridge deck and two accelerometers of type PCB 393b31 (10 V/g) were placed at the bridge supports. Two types of excitation sources were applied during the experiments: impulse and slow sine excitation. A Dytran impulse hammer model 5803A was used to provide a transient impulse force of around 10 kN. The subsequent free vibration of the bridge was thereafter recorded. A soft hammer tip was chosen in order to excite frequencies in the low frequency range. In order to reduce the influence of noise, approximately 10 hits were recorded at each excitation point in order to perform an average when producing frequency response functions and achieve good coherence. Slow sine testing with a force of 75 N and a linearly increasing speed of around 0.01-0.02 Hz/s was achieved with an electrodynamic shaker of type BD-5 from Wölfel Monitoring Systems. Two accelerometers were placed on the shaker: one PCB 393a03 at the platform and one PCB308B (0.1 V/g) on the moving mass. The amplification of the signals and conversion from analogue to digital signals was achieved with the data acquisition system QuantumX by HBK (former HBM) with one MX1601B and two MX840B modules. The accompanying software Catman®Easy version 5.3.1 was used to store the data. In order to determine the average temperature of the asphalt layer, an infrared thermometer

of type Testo 830-T2 was utilized. The surface temperature was measured at a few points on the bridge deck and at a couple of time instants during the measurements.

2.3 Instrumentation

The bridge was experimentally tested during four different construction stages, see Figure 3:

Stage 1) Timber structure including longitudinal beams, SLT deck and crossbeams.
Stage 2) Timber structure and railings.
Stage 3) Timber structure, railings and asphalt during warm conditions.
Stage 4) Timber structure, railings and asphalt during cold conditions.

Figure 3: The bridge during and after construction. Left: Stage 1 with only the timber structure. The vertical flat bars for the railings were present on the bridge. Right: Finished bridge (stage 3 and 4) with timber structure, railings and asphalt.

The instrumentation setup for the measurements, see Figure 4, were identical for the different construction stages with 14 vertical (a_{V1}-a_{V14}) and 5 lateral (a_{L1}-a_{L5}) accelerometers on the bridge deck as well as 2 axial (a_{A1}-a_{A2}) accelerometers at the bridge supports. Six excitation points were chosen on the bridge in order to obtain a sufficient number of vibration modes. Hammer excitation was applied at each excitation point. Slow sine tests were applied at positions E2 and E5 in order to excite the first bending and torsional mode.

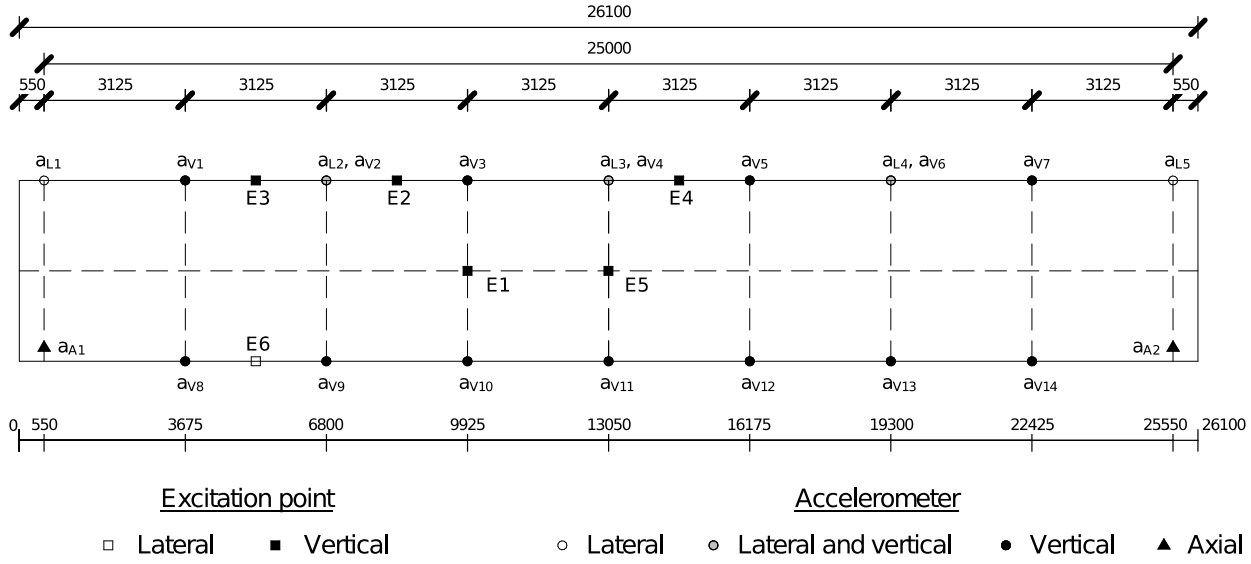

Figure 4: Instrumentation setup for the experiments. The white, grey and black circles indicate if a vertical, lateral or both lateral and vertical accelerometer exist on the position. The black triangles indicate the locations of the axial accelerometers at the bridge supports. The white and black boxes indicate if it is a lateral or vertical excitation point.

2.4 Post-processing

This section describes the post-processing which includes frequency response functions as well as the coherence function, mode indicator function and modal assurance criterion.

2.4.1 Frequency response function

The frequency response function (FRF) was calculated as the H_1-estimator in Equation 2-1, which assumes that the input signal is known and that only the output signal contains noise. It is determined by applying fast Fourier transform (FFT) on both input and output signals, resulting in $X(f)$ for the input and $Y(f)$ for the output signal. Both results are thereafter multiplied with the complex conjugate of the input signal's FFT, $X^*(f)$. Averaging these quantities for N measurements results in $\hat{S}_{yx}(f)$ and $\hat{S}_{xx}(f)$ in Equation 2-1, which are the averaged cross- and auto-spectral densities respectively. The H_1-estimator assumes that enough averages are made such that the uncorrelated noise in the output signals becomes small enough to neglect [8].

$$\widehat{H}_1(f) = \frac{\frac{1}{N}\sum_{i=1}^{N} Y_i(f)X_i^*(f)}{\frac{1}{N}\sum_{i=1}^{N} X_i(f)X_i^*(f)} = \frac{\hat{S}_{yx}(f)}{\hat{S}_{xx}(f)} \qquad 2\text{-}1$$

2.4.2 Coherence function

To validate the quality of the FRFs, the coherence function ($\hat{\gamma}_{yx}^2$) in Equation 2-2 can be applied.

$$\hat{\gamma}_{yx}^2(f) = \frac{\widehat{H}_1(f)}{\widehat{H}_2(f)} = \frac{\left|\hat{S}_{yx}(f)\right|^2}{\hat{S}_{xx}(f)\hat{S}_{yy}(f)}, \qquad 0 \le \hat{\gamma}_{yx}^2(f) \le 1 \qquad 2\text{-}2$$

The coherence function calculates the ratio between the H_1- and H_2-estimator. The H_2-estimator assumes, contrary to the H_1-estimator, that noise is only present in the input signal. The average $\widehat{H}_2$-estimator based on N measurements can be seen in Equation 2-3.

$$\widehat{H}_2(f) = \frac{\frac{1}{N}\sum_{i=1}^{N} Y_i(f)Y_i^*(f)}{\frac{1}{N}\sum_{i=1}^{N} X_i(f)Y_i^*(f)} = \frac{\hat{S}_{yy}(f)}{\hat{S}_{xy}(f)} \qquad 2\text{-}3$$

Since H_1 contains noise in the numerator and H_2 in the denominator, the true function H must exist somewhere in the range stated in Equation 2-4. A value of $\hat{\gamma}_{yx}^2 = 1$ indicates therefore that $\widehat{H}_1 = \widehat{H}_2$ and that there is no noise present in the signals [8].

$$\left|\widehat{H}_1(f)\right| \le |H(f)| \le \left|\widehat{H}_2(f)\right| \qquad 2\text{-}4$$

2.4.3 Mode indicator function

To determine the resonance frequencies correctly, the mode indicator function (MIF) in Equation 2-5 can be established. There exists several MIFs, and in this work the "normal MIF" or "MIF 1" is utilized. The MIF for n accelerometers is defined as a sum of the real part of the FRFs divided by the magnitude of the FRFs at each frequency. Since the FRF is mainly real-valued except at an undamped eigenfrequency where it is imaginary, the MIF will be approximately 1 for all frequencies except at an eigenfrequency where it dips towards zero [8].

$$\mathrm{MIF}(f) = \frac{\sum_{i=1}^{n}\left|\mathrm{Re}\left[\widehat{H}_{1,i}(f)\right]\right|^2}{\sum_{i=1}^{n}\left|\widehat{H}_{1,i}(f)\right|^2}, \qquad 0 \le \mathrm{MIF}(f) \le 1 \qquad 2\text{-}5$$

2.4.4 Modal assurance criterion

To validate the modes of vibration, the modal assurance criterion (MAC) in Equation 2-6 can be implemented. This method compares the similarity between two mode vectors and produces a value between 1 and 0. A value closer to 1 indicates a greater similarity and vice versa. When comparing more than one mode a MAC matrix is produced where the value $\mathrm{MAC}(m,n)$ is the comparison of mode vector ϕ_m and ϕ_n at row m and column n.

$$\mathrm{MAC}(m,n) = \frac{|\{\phi_m\}^T\{\phi_n\}|^2}{(\{\phi_m\}^T\{\phi_m\})(\{\phi_n\}^T\{\phi_n\})} \qquad 2\text{-}6$$

The auto-MAC is a comparison between the same set of modes, which is an indicator of how well separated they have been established from the measurements. The degree of separation depends greatly on the number of measurement positions during the experiments. The cross-MAC is a comparison between two different sets of mode, for example numerical and experimental modes [8]. In this work auto-MAC is established for the individual experiments and cross-MAC between modes for stage 1 and stages 2-4 to ensure that the same modes are compared and evaluated.

2.5 Modal parameter extraction

The FRFs were thereafter analysed with two different modal parameter extraction methods: the complex exponentials method and a single degree of freedom method. Resonance frequencies and damping ratios were retrieved with both methods, whereas the mode shapes were only retrieved with the complex exponentials method.

2.5.1 Complex exponentials method

The complex exponentials (CE) method expresses the FRF on pole-residue form, see the receptance based on displacement $X(s)$ with the Laplace variable s in Equation 2-7. A summation of P number of poles is expressed in the equation and out-of-bounds modes are not considered. The subscripts i and j denotes accelerometer i and excitation point j. The real part of the poles (s_n) represents the damping and the imaginary part represents the resonance frequency. The real part of the residues ($_nR_{ij}$) represent the phase angle and the imaginary part represents the amplitude for the mode of vibration. Poles and residues come in complex conjugate pairs to represent both the negative and positive imaginary axis. Derivations of the CE method can be found in literature [9].

$$H_{ij}(s) = \frac{X_i(s)}{F_j(s)} = \sum_{n=1}^{P}\left(\frac{{}_nR_{ij}}{s-s_n} + \frac{{}_nR_{ij}^*}{s-s_n^*}\right) \qquad 2\text{-}7$$

2.5.2 Single degree of freedom method

The single degree of freedom (SDOF) method assumes that each resonance peak can be approximated as an oscillating mass-spring-damper system with a single degree of freedom. The accelerance function based on acceleration $A(\omega)$ expressed with the stiffness k, angular frequency ω and natural frequency ω_n is presented in Equation 2-8 [8]. A curve-fitting procedure estimating the coefficients in the denominator polynomial in Equation 2-8 for each resonance peak individually gives an approximation of the modal parameters.

$$|H(\omega)| = \left|\frac{A(\omega)}{F(\omega)}\right| = \frac{\omega^2/k}{\sqrt{\left(1-\left(\frac{\omega}{\omega_n}\right)^2\right)^2 + \left(2\zeta\frac{\omega}{\omega_n}\right)^2}} \qquad 2\text{-}8$$

3 Results

This section presents the experimental results, i.e. the modes of vibration, resonance frequencies and damping ratios. Numerical results from an FE model are also presented.

3.1 Experimental results

The average air temperature during the construction stages were: 1) 12.6 ºC, 2) 5.5 ºC, 3) 21.4 ºC and 4) -0.8 ºC. The average relative humidity was: 1) 57 %, 2) 48 %, 3) 58 % and 4) 70 %. The average temperature of the asphalt layer was 41.9 ºC during stage 3 and 0.6 ºC during stage 4. The mechanical properties of timber are not significantly affected by temperature in the normal range of -30 ºC to 90 ºC [1]. The asphalt stiffness is however largely affected by temperature. The varying stiffness of asphalt can be found in several other previous studies with a value of the modulus of elasticity (MOE) of around 0.5-1.5 GPa at 40 ºC and 15-20 GPa at 0 ºC [10]–[12].

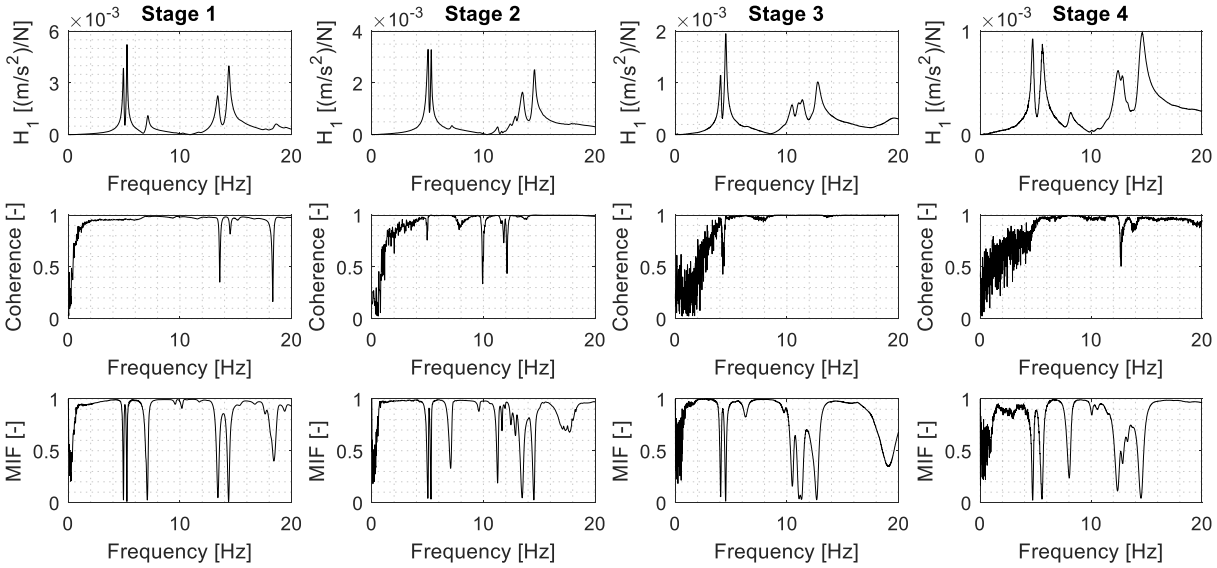

Figure 5: Hammer excitation at excitation point E2. H_1-estimator, coherence and MIF between 0-20 Hz for accelerometer a_{V3} at construction stages 1-4.

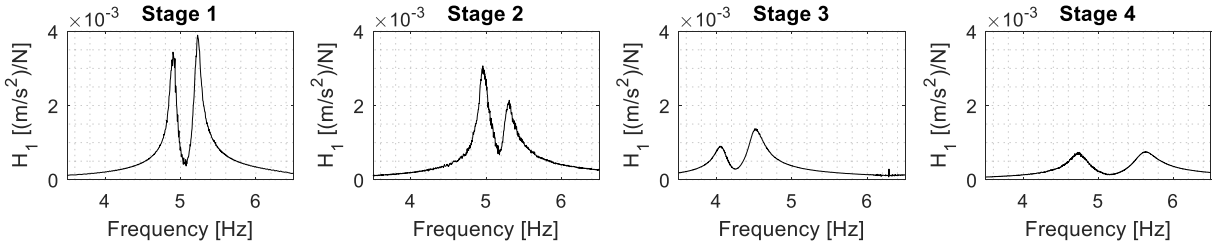

Figure 6: Slow sine excitation at excitation point E2. H_1-estimator between 3.5-6.5 Hz for accelerometer a_{V3} at construction stages 1-4. The resonance peaks for the first bending and torsional mode are well-defined.

The H_1-estimator, coherence and MIF for construction stages 1-4 are presented in Figure 5. The excitation point is E2 with impulse hammer and accelerometer a_{V3} is evaluated for the FRF and coherence. The MIF is however evaluated for all accelerometers in order to determine the resonance frequencies correctly. The coherence indicate well-established FRFs with a value close to 1 at the resonance peaks. The FRFs at stages 1-4 for accelerometer a_{V3} from slow sine excitation at excitation point E2 between 3.5 to 6.5 Hz are presented in Figure 6. The first bending and torsional mode are excited.

3.1.1 Modes of vibration

The first six modes of vibration for the bridge can be seen in Figure 7. The modes are abbreviated according to their shape with bending (B), torsion (T) and lateral (L). They are also ordered numerically (1, 2 …) within their category.

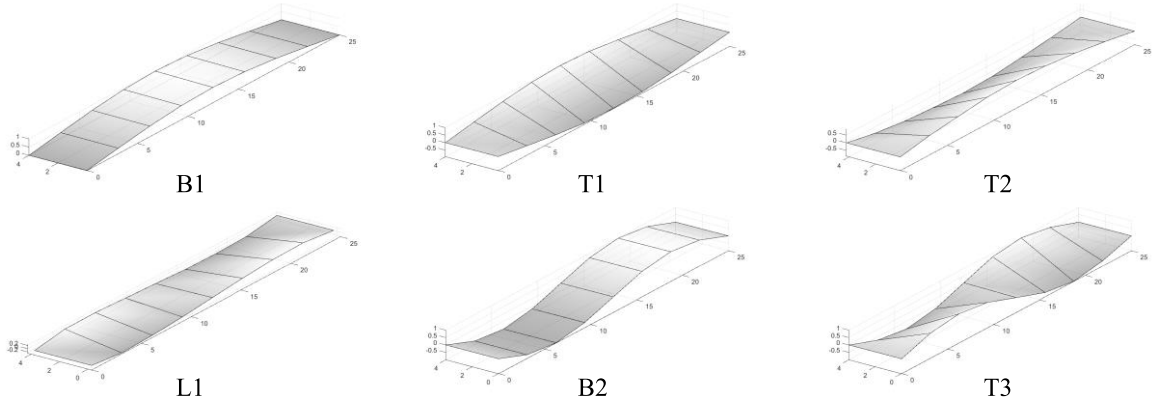

Figure 7: The first six vibration modes for the bridge.

The auto-MAC was established for the individual experiments in order to distinguish how well separated the modes are, see Figure 8. All diagonal values are 1 since the mode is compared with itself. T1 and T2 as well as L1 and T3 are quite similar but the lateral components for T2 and L1 are much larger than for T1 and T3. An increased number of measurement points would be needed to separate them more. It is however assumed that they are sufficiently separated to be able to compare them with numerical modes for example. The cross-MAC, i.e. comparison between two different set of modes, is established to verify that the same modes are chosen for all experiments, see Figure 9. The modes for stage 1 are therefore compared with the modes for construction stages 2-4. It can be seen that the current cross-MAC values are between 0.74-1 on the diagonals which provides a good validation.

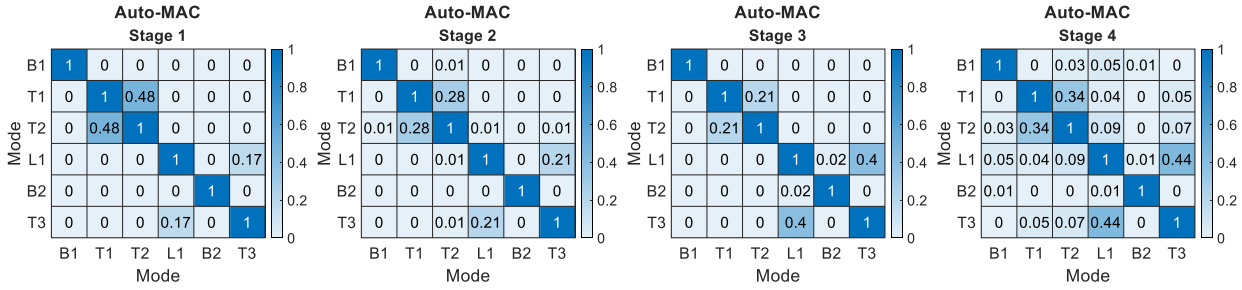

Figure 8: Auto-MAC for construction stages 1-4.

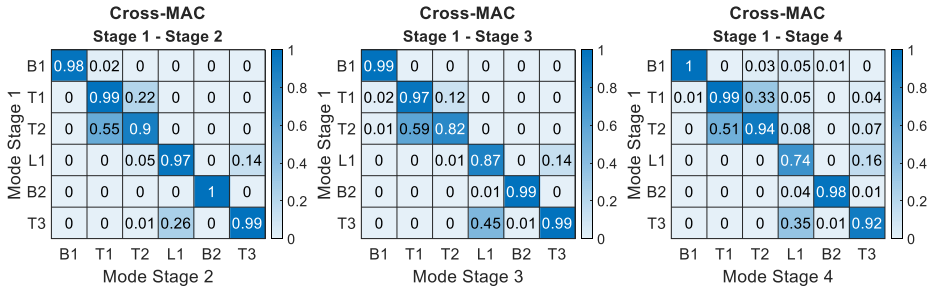

Figure 9: Cross-MAC between construction stage 1 and stages 2-4.

Table 1: Resonance frequencies for the construction stages.

	Resonance frequencies [Hz]					
Stage	**B1**	**T1**	**T2**	**L1**	**B2**	**T3**
Stage 1	4.93	5.24	7.11	9.65	13.41	14.37
Stage 2	5.03	5.31	7.16	9.65	13.52	14.56
Stage 3	4.07	4.52	6.33	9.81	10.52	12.72
Stage 4	4.74	5.58	8.05	11.45	12.37	14.54

3.1.2 Resonance frequencies and damping

The resonance frequencies for each construction stage can be seen in Table1. The resonance frequencies are increased with 0-2 % at stage 2 when railings are present on the bridge. This is most likely due to an overall higher stiffness compared to its mass as well as the continuity of the railings beyond the bridge deck boundaries. If only the mass of the railings is considered, which is around 5 % of the bridge's total mass (10 % if the vertical flat bars for the railings from stage 1 is included, see Figure 3), B1 would be decreased to around 4.81 Hz. The increase to 5.03 Hz with railings must therefore mean that the stiffness is increased with around 10 % for B1. L1 is not changed however which means that the added mass and stiffness cancel each other out laterally. Adding an asphalt layer on the bridge at stage 3 can be seen to lower all vertical resonance frequencies with 12-22 %, which is expected since the temperature of the asphalt layer was around 41.9 ºC. The asphalt is expected to mainly increase the mass of the bridge and not the stiffness since asphalt has a low MOE at high temperatures. However, L1 is increased with 2 % at stage 3 compared to stage 2. This is probably due to the asphalt layer's second moment of area which is approximately $3 \cdot 10^3$ larger in the lateral direction compared to the vertical direction. The resonance frequencies increased with 14-27 % at stage 4 compared to stage 3. This is probably due to the asphalt's higher stiffness at a low temperature of around 0.6 ºC. B1 and B2 at stage 4 are not larger than B1 and B2 at stage 2. However, T3 is similar and both T1 and T2 are larger at stage 4 as compared to stage 2. This indicates that the asphalt increases the torsional stiffness of the bridge substantially. A larger decrease in the resonance frequencies for bending modes compared to torsional modes can also be seen between stage 2 and 3.

The damping ratios for the different construction stages depending on type of excitation and modal parameter extraction method are presented in Table 2. They are evaluated for all excitation points when applicable and the average (μ) damping ratios and standard deviations (σ) are presented. Average values based on both modal parameter extraction methods and excitation types are also presented. The damping ratios for the finished bridge with asphalt are around 2-3 %, which fall in the normal range of pedestrian bridges of around 1-3 % [2], [3], [5], [13]. The damping ratio for timber bridges is set to 1-1.5 % in EN-1995-2, which may be regarded as conservative [14]. Both railings and asphalt increase the damping ratio. The damping with an asphalt layer is increased during cold compared to warm conditions which could be due to increased friction at the interface between timber deck and asphalt. An effective way of adding damping to the bridge is therefore to add asphalt, which is confirmed by previous studies [6], [7]. The values of the standard deviations can be seen to be quite small which reinforces the reliability of the damping ratios, except when the damping is only evaluated for one excitation point. The two different modal parameter extraction methods can be seen to produce similar values which ensures their reliability. The two types of excitation, i.e. impulse and slow sine excitation, also produce similar values.

*Table 2: Damping ratios in percent for the construction stages. The values are presented as "μ (σ)", where μ is the mean value and σ is the standard deviation. All excitation points are included in the results when applicable. * σ is only based on one value due to limited ability for parameter extraction in this particular case. The rows with "Average" presents the average values based on both modal parameter extraction methods and excitation types.*

			Damping ratios [%]					
Stage	**Excitation**	**Method**	**B1**	**T1**	**T2**	**L1**	**B2**	**T3**
Stage 1	**Hammer**	**CE**	1.09 (0.12)	0.88 (0.02)	1.47 (0.01)	1.14 (0.00*)	1.20 (0.13)	0.84 (0.04)
		SDOF	1.04 (0.10)	0.84 (0.02)	1.47 (0.02)	1.17 (0.00*)	1.13 (0.09)	0.85 (0.01)
	Sweep	**CE**	0.94 (0.18)	0.87 (0.09)				
		SDOF	1.01 (0.14)	0.97 (0.10)				
		Average	1.04	0.88	1.47	1.16	1.17	0.84
Stage 2	**Hammer**	**CE**	1.54 (0.13)	1.07 (0.14)	2.05 (0.09)	1.24 (0.00*)	1.63 (0.15)	0.84 (0.05)
		SDOF	1.42 (0.16)	1.03 (0.01)	1.87 (0.07)	1.30 (0.00*)	1.51 (0.09)	0.91 (0.01)
	Sweep	**CE**	1.07 (0.08)	1.09 (0.01)				
		SDOF	1.15 (0.02)	1.27 (0.14)				
		Average	1.37	1.10	1.96	1.27	1.57	0.88
Stage 3	**Hammer**	**CE**	1.81 (0.06)	1.86 (0.08)	5.07 (0.00*)	2.01 (0.00*)	1.63 (0.02)	1.89 (0.06)
		SDOF	1.93 (0.18)	1.90 (0.01)	4.62 (0.00*)	1.93 (0.00*)	1.73 (0.11)	1.91 (0.01)
	Sweep	**CE**	2.06 (0.03)	2.14 (0.02)				
		SDOF	2.06 (0.00)	2.33 (0.00*)				
		Average	1.96	2.03	4.85	1.97	1.72	1.90
Stage 4	**Hammer**	**CE**	2.72 (0.15)	2.78 (0.21)	2.85 (0.29)	2.74 (0.00*)	2.53 (0.10)	2.16 (0.24)
		SDOF	2.60 (0.15)	3.17 (0.20)	2.57 (0.11)	2.29 (0.00*)	2.65 (0.24)	2.07 (0.01)
	Sweep	**CE**	2.48 (0.03)	2.95 (0.00*)				
		SDOF	2.80 (0.07)	3.05 (0.03)				
		Average	2.65	2.97	2.66	2.52	2.59	2.12

3.1.3 Boundary conditions

A figure of the bridge supports is presented in Figure 10. The bolt hole is circular at accelerometer a_{A2} whereas it is oval at accelerometer a_{A1} to allow for expansion of the timber due to temperature and moisture.

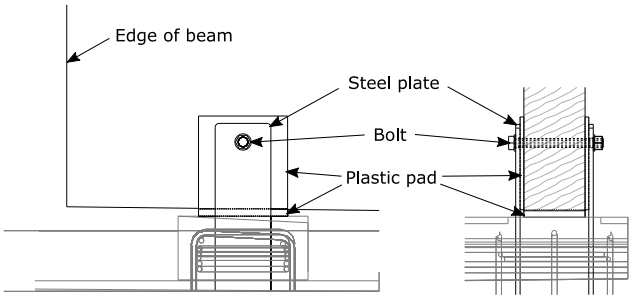

Figure 10: Bridge support. Left: View from the side. Right: Cross-sectional view.

Accelerometers a_{A1} and a_{A2} show that the bridge bolts have free axial translation for bending modes, whereas a_{A1} have free and a_{A2} have restricted translations for torsional modes due to the differences of the bolt holes, see Figure 11.

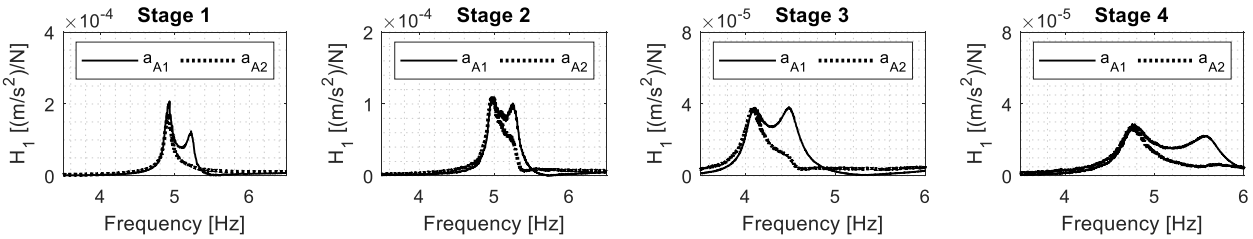

Figure 11: Slow sine excitation at excitation point E2. H_1-estimator between 3.5-6.5 Hz for accelerometers a_{A1} and a_{A2} at the bridge supports. The resonance peaks for the first bending and torsional mode can be seen for a_{A1} but only the first bending mode for a_{A2}.

3.2 Numerical results

An FE model is made in MATLAB with 2D Euler-Bernoulli beam elements with isotropic material elasticity. The length of the beam is increased from 26.1 to 26.2 m to simplify the modelling, has supports at 0.6 m from the beam edges and a beam element length of 0.2 m, see Figure 12. The vertical translations are restricted and the axial translations are free at the bridge boundary conditions in accordance to Section 3.1.3. Since the bridge supports are at the bottom edge of the longitudinal beams, the degrees of freedom are translated a distance *e* from the centre of gravity to this position in the model. The timber MOE is set to 12500 MPa and the density is set to 475 kg/m^3. The values are retrieved from two studies: one by the Scandinavian company Moelven and another by Jockwer [15]. Both studies performed tests on samples of class GL30c or equivalent with a moisture content of 12 %. Both values are close to the ones found in EN-14080, but the applied values could be more reasonable based on experience gained by the authors' previous research. The asphalt density is set to 2450 kg/m^3 since normal values are between 2400-2500 kg/m^3 [1]. It is also noted that the results only differ around 1 % within this range. The value of 2450 kg/m^3 is similar compared to previous experimental studies [16]–[18]. The asphalt MOE is estimated to 1 GPa during warm and 17 GPa during cold conditions from previous studies such as [10]–[12]. The asphalt and timber deck is assumed to act as a beam with full composite action where the asphalt cross-section is transformed to an equivalent timber cross-section. The railings are neglected in the model.

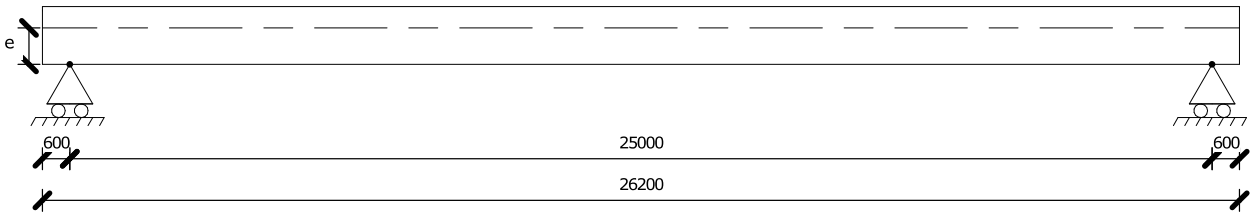

Figure 12: 2D beam model of the bridge with supports at the bottom of the beam at a distance e from the centre of gravity (dashed line). Dimensions are in mm.

The results for the first two bending modes for stage 1, 3 and 4 are presented in Table 3. Stage 2 is not included since there is only a slight difference in the experimental results between stage 1 and 2. The numerical results for B1 are lower than the experimental results and no reasonable change in the material parameter values can be applied to come closer to the experimental values. This indicates that there is a lack of stiffness for B1 in the FE model which could be explained by shear deformation of the plastic pads underneath the longitudinal beams which is neglected in the model. In fact, introducing a spring at both supports in the FE model increases B1 but not B2.

Table 3: Experimental and numerical results for the first two bending modes for stages 1, 3 and 4. All values are in hertz (Hz).

	Stage 1		**Stage 3**		**Stage 4**	
	Exp.	**Num.**	**Exp.**	**Num.**	**Exp.**	**Num.**
B1	***4.93***	4.19	***4.07***	3.17	***4.74***	3.53
B2	***13.41***	16.77	***10.52***	12.66	***12.37***	14.12

4 Conclusions

This article evaluates the dynamic properties of a timber pedestrian bridge. Dynamic tests were performed at four different construction stages: 1) on only the timber structure 2) on the timber structure with the railings 3) on the timber structure with railings and an asphalt layer during warm conditions and 4) same as stage 3 but during cold conditions. The modes of vibration, resonance frequencies and damping ratios were retrieved by modal parameter extraction for all stages. A 2D FE model was thereafter implemented and numerical results were retrieved for stage 1, 3 and 4. The following conclusions can be derived:

- The stiffness of the railings contribute more than the railing mass to the resonance frequencies at stage 2 compared to stage 1. The first bending mode is increased from 4.93 to 5.03 Hz and would theoretically be decreased to around 4.81 Hz if only the railing mass would be considered. This means that the railings increases the stiffness of the first bending mode with around 10 %.
- The effect of the asphalt during warm conditions is mainly to add mass to the vertical bending and torsional resonance frequencies which are lower in stage 3 compared to stage 2. This is the opposite for the first lateral mode where the resonance frequency is higher in stage 3 compared to stage 2. This is probably due to a large increase in the second moment of area in the lateral direction due to the presence of the asphalt layer.
- The resonance frequencies at stage 4 (cold conditions) are higher compared to stage 3 (warm conditions). This is probably due to the increase of the asphalt stiffness at cold conditions. It can also be observed that the resonance frequencies are lower for the bending modes but higher for the torsional modes at stage 4 compared to stage 2.
- Damping is increased for each construction stage and the final values are in the normal range of approximately 2-3 %. The asphalt increases the damping and is a good way to increase the damping of pedestrian bridges. The damping is also increased during cold (stage 4) compared to warm conditions (stage 3).
- Both the auto-MAC and cross-MAC values are consistent for the modes of vibration for all construction stages.
- The CE and SDOF method produce similar results and the results are therefore reliable. It should therefore be possible to achieve results for resonance frequencies and damping ratios with only one of these methods.
- The FE model shows large differences from the experimental results. It appears that some stiffness is lacking for the first bending mode. This stiffness could be due to shear deformation of the plastic pads at the bridge supports. Further modelling with a 3D orthotropic numerical model is suggested.

Acknowledgement

This project is funded by the Swedish Transport Administration and the J Gustaf Richerts foundation. The authors gratefully recognize these contributions. The authors also want to thank the companies Moelven and Skanska for all help with the dynamic measurements on-site and for providing constructional drawings of the bridge. The authors also want to thank the municipality in Växjö, Sweden, for providing information and help.

References

[1] Swedish Wood, *Design of timber structures. Volume 1 - Structural aspects of timber construction.* Swedish Wood, 2019.

[2] J. H. Neilson *et al.*, “Experimental and Numerical Dynamic Properties of Two Timber Footbridges Including Seasonal Effects,” *Int. J. Civ. Eng.*, vol. 19, no. 10, pp. 1239–1250, 2021.

[3] R. Castro-Triguero, E. Garcia-Macias, E. S. Flores, M. I. Friswell, and R. Gallego, “Multi-scale model updating of a timber footbridge using experimental vibration data,” *Eng. Comput. (Swansea, Wales)*, vol. 34, no. 3, pp. 754–780, 2017.

[4] A. Gheitasi, O. E. Ozbulut, S. Usmani, M. Alipour, and D. K. Harris, “Experimental and analytical vibration serviceability assessment of an in-service footbridge,” *Case Stud. Nondestruct. Test. Eval.*, vol. 6, pp. 79–88, 2016.

[5] C. Heinemeyer and M. Feldmann, "European design guide for footbridge vibration," *Footbridge Vib. Des.*, pp. 13–30, 2009.

[6] S. Schubert, D. Gsell, R. Steiger, and G. Feltrin, "Influence of asphalt pavement on damping ratio and resonance frequencies of timber bridges," *Eng. Struct.*, vol. 32, no. 10, pp. 3122–3129, Oct. 2010.

[7] Glauco Feltrin, Sandy Schubert, and René Steiger, "Temperature effects on the natural frequencies and modal damping of timber footbridges with asphalt pavement," 2011.

[8] A. Brandt, *Noise and vibration analysis signal analysis and experimental procedures*. Chichester, West Sussex, U.K. ; Hoboken, N.J.: Wiley, 2011.

[9] N. Maia, "Extraction of valid modal properties from measured data in structural vibrations," 1989.

[10] Y. Zhao, J. Tang, and H. Liu, "Construction of triaxial dynamic modulus master curve for asphalt mixtures," *Constr. Build. Mater.*, vol. 37, pp. 21–26, 2012.

[11] P. Pokorski, P. Radziszewski, and M. Sarnowski, "Rheological properties of asphalt mixtures for bridge pavements," *Procedia Eng.*, vol. 111, no. TFoCE, pp. 637–644, 2015.

[12] M. Halle, T. Rukavina, and J. Domitrovic, "Influence of temperature on asphalt stiffness modulus," *5th Eurasphalt Eurobitume Congr. 13-15th June 2012, Istanbul*, no. June 2012, pp. 13–15, 2012.

[13] K. Van Nimmen, "Numerical and Experimental Study of Human-Induced Vibrations of Footbridges." 2015.

[14] Swedish Standards Institute, "Swedish standard SS-EN 1995-2:2004. Eurocode 5: Design of timber structures – Part 2: Bridges," Stockholm, 2009.

[15] R. Jockwer, "Structural behaviour of glued laminated timber beams with unreinforced and reinforced notches," 2014.

[16] A. Baltrušaitis, A. Vaitkus, and J. Smirnovs, "Asphalt layer density and air voids content: GPR and laboratory testing data reliance," *Balt. J. Road Bridg. Eng.*, vol. 15, no. 3, pp. 93–110, 2020.

[17] C. E. Sengul, S. Oruc, E. Iskender, and A. Aksoy, "Evaluation of SBS modified stone mastic asphalt pavement performance," *Constr. Build. Mater.*, vol. 41, pp. 777–783, 2013.

[18] A. Chegenizadeh, B. Peters, and H. Nikraz, "Mechanical properties of stone mastic asphalt containing high-density polyethene: An Australian case," Case Stud. Constr. Mater., vol. 15, no. May, p. e00631, 2021.